Journal of Applied Fluid Mechanics, Vol. 11, No. 3, pp. 667-678, 2018.
Available online at www.jafmonline.net, ISSN 1735-3572, EISSN 1735-3645.
DOI: 10.29252/jafm.11.03.27778

Electroosmotic Pumping Between Two Immiscible Electrical Conducting Fluids Controlled by Interfacial Phenomena

A. Matías[1], O. Bautista[2†] F. Méndez[1] and P. Escandón[2]

[1] *Departamento de Termofluidos, Facultad de Ingeniería, UNAM, México City, 04510, Mexico*
[2] *ESIME Azcapotzalco, Instituto Politécnico Nacional, México City, 02250, Mexico*

†Corresponding Author Email: obautista@ipn.mx

(Received March 14, 2017; accepted December 23, 2017)

ABSTRACT

In this study, the isothermal electroosmotic flow of two immiscible electrical conducting fluids within a uniform circular microcapillary was theoretically examined. It was assumed that an annular layer of liquid adjacent to the inside wall of the capillary exists, and this in turn surrounds the inner flow of a second liquid. The theoretical analysis was performed by using the linearized Poisson-Boltzmann equations, and the momentum equations for both fluids were analytically solved. The interface between the two fluids was considered uniform, hypothesis which is only valid for very small values of the capillary number, and shear and Maxwell stresses were considered as the boundary condition. In addition, a zeta potential difference and a charge density jump were assumed at the interface. In this manner, the electroosmotic pumping is governed by the previous interfacial effects, a situation that has not previously been considered in the specialized literature. The simplified equations were nondimensionalized, and analytical solutions were determined to describe the electric potential distribution and flow field in both the fluids. The solution shows the strong influence of several dimensionless parameters, such as μ_r, ε_r, $\bar{\zeta}_w$, $\Delta\bar{\psi}$ and $\bar{Q}_{sf}$, and $\bar{\kappa}_{1,2}$, on the volumetric flow. The parameters represent the ratio of viscosity, the ratio of electric permittivity of both fluids, the dimensionless zeta potential of the microcapillary wall, the dimensionless charge density jump and charge density between both fluids, and the electrokinetic parameters, respectively.

Keywords: Immiscible conducting fluids; Electroosmosis; Circular microcapillary; Maxwell stress; Interfacial stress.

1. INTRODUCTION

Micro- and nanofabricated devices have led to revolutionary changes in the ability to manipulate tiny volumes of fluids or micro- and nanoparticles contained within the fluids. This has led to the development of applications in chemical and particulate separation and analysis, biological characterization, sensors, cell capture and counting, micropumps and actuators, high-throughput design and parallelization, and system integration (Kirby 2010). Electroosmotic pumping based on the phenomenon of electroosmosis can be used to accomplish tasks involving the manipulation of tiny volumes of fluids. It refers to the motion of an electrolytic fluid relative to a stationary charged surface when an electric field is applied (Probstein 2005). However, electroosmosis cannot be directly used to drive noncon-ducting liquids or liquids with very low conductivity such as oil, ethanol, and blood. In this context, Brask *et al.* (2003) proposed an electroosmotic pump that relied on two liquids with different viscosities. The pump supplied nonconducting liquids or liquids with very low conductivity when a con-ducting pumping liquid driven by EOF dragged a nonconducting liquid by means of viscous forces. Hence, an increasing amount of attention was focused on the study of electrokinetic flows for multiphase systems containing liquid-liquid interfaces subject to electric fields.

The pumping of non-conducting fluids has widely analyzed in several previous studies (Brask *et al.* 2003; Choi *et al.* 2011; Movahed *et al.* 2012; Matías *et al.* 2017; Qi and Ng 2018). Gao *et al.*(2005) proposed an approach in which high elec-troosmotic mobility liquid was used as a driving mechanism to drag the low electroosmotic mobility liquid. Choi *et al.* (2011) studied a two-fluid electroosmotic flow in a microchannel based on full

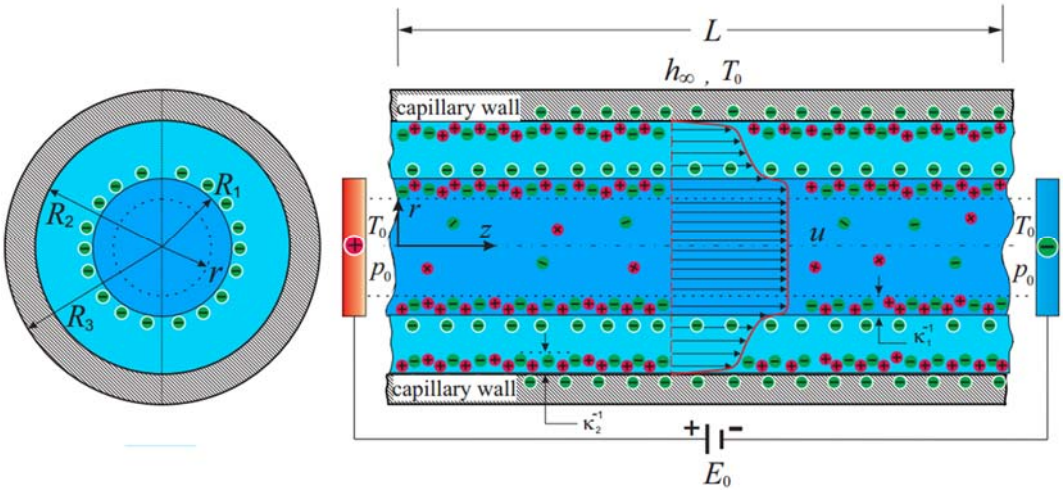

Fig. 1. Sketch of the electroomostic flow of two immiscible and symmetric (z : z) electrolyte solutions with an annular arrangement.

hydrodynamic and electrostatic interactions on the liquid-liquid interface in which the inter-facial electrostatic effects were shown. Su *et al*.(2013) obtained semi-analytical solutions for transient electroosmotic and pressure-driven flows of two-layer fluids between microparallel plates in which Maxwell stress at the interface was included. A numerical simulation of the electroosmotic flow in a column of an aqueous solution surrounded by an immiscible liquid was examined by Movahed *et al*. (2012). Their results indicated effects on the flow field of ζ -potential and viscosity ratio of the two fluids. Liu *et al*. (2009) presented a numerical study for a circular two-phase electroosmotic flow that involved pumping a conducting peripheral layer of fluid that dragged the inner fluid. In the same direction, Jabari (2016) analyzed the flow of two immiscible fluids in a circular microchannel. He considered that the inner fluid is a non-conducting liquid and the surrounding liquid is conductive, where the former is driven by pressure forces and the latter is driven by electroosmotic forces. In addition, electric double layers form at the wall as well as at the liquid-liquid interface, which are in contact with the high EO mobility liquid. However, in such analysis, it is assumed the non-existence of a zeta potential difference, as well as a surface charge at the interface between both fluids. The two aspects mentioned before are considered in the present work.

Conversely, it was observed that an electric field can penetrate a conductive dielectric liquid. This leads to the formation of double layers on both sides of the interface (Pascall and Squires 2011). Verway and Niessen (1939) were the first to de-scribe the electrical double layer at the interface of two immiscible electrolyte solutions as two non-interacting diffuse layers with a layer on each side of the interface. Volkov *et al*. (1996) presented an excellent review on the status of the theory with respect to the electrical double layer at a liquid/liquid interface.

The electrical double layer at the oil/water interface is a heterogeneous interfacial region that separates two bulk phases of polarized media and maintains a spatial separation of charges (Volkov *et al*. 1996). Thus, there are frequent occurrences of liquids that are electrically weak conductors. However, the EDL is formed at the interface between the two fluids. In this context, most theoretical and numerical studies on two-liquid electroosmotic flows in microchannels were conducted in Cartesian coordinates and do not show the effect of the EDLs formed at the interface between the fluids. In this aspect, the present study derived an analytical solution of the electroosmotic flow by accounting for electrokinetic effects at solid-liquid and liquid-liquid interfaces. Specifically, electrical and viscous stresses were considered at the liquid-liquid interface. The results of the analysis revealed the importance of the formation of the EDL at the interface between both immiscible fluids as well as the physical properties of the fluids.

2 PROBLEM DEFINITION

Figure 1 shows the scheme of the physical model analyzed in this study. A microcapillary with length L that considerably exceeded its inner radius R_2 was filled with two immiscible and symmetric (z : z) electrolyte solutions with an annular arrangement. A 2D cylindrical coordinate system (r,x) was adopted, and the origin was placed at the left end of the capillary tube. The column of the inner fluid had a radius of R_1. The flow was exclusively driven by the effect of electro-osmotic forces originating in an electric field externally applied in the x axial direction with an intensity of $E_0 = \varphi_0/L$, in which φ_0 denotes the value of the electric potential imposed at the entrance of the microcapillary, i.e., at x = 0. At the interface between both fluids, a zeta potential difference and Maxwell stress were considered.

Additionally, the following assumptions are made:(i) Debye lengths at the interface between both fluids and at the liquid-wall interface as denoted by $\lambda_{D,i}$ or κ_i^{-1} were very small, where the subscript i = 1,2 denotes the inner and surrounding fluids,

respectively, and it was defined as $\lambda_{D,i} = \kappa_i^{-1} = (\varepsilon_i k_B T / 2e^2 z_i^2 n_{\infty,i})$. Here, ε_i, k_B, T , e, and z_i and $n_{\infty,i}$ denote dielectric permittivity of the two electrolytes, Boltzmann constant, absolute temperature, elementary charge, and valence and bulk concentrations, respectively, for both fluids. The Debye lengths were assumed as very small, i.e., $\kappa_1^{-1} \ll R_1$ and $\kappa_2^{-1} \ll h$, where $h = R_2 - R_1$. (ii) The interface between the two fluids was well defined and stable. i.e., the liquid film thickness h was constant along the microcapillary. In this context, the very small pressure difference that arose from surface tension and curvature was ignored (Middleman 1995). This is a restrictive assumption, however, we assume that the interface remains stable because the capillary number, is very small, i.e., $Ca = \varepsilon E_0 \psi_c / \gamma_T \ll 1$ (Mandal *et al*. 2015); for instance, typical values of the physical parameters used in this study take the following values: the dielectric permittivity is $\varepsilon \sim 7 \times 10^{-10}$ C V^{-1} m^{-1}, the external electric field $E_0 \sim 10^4$ V m−1, the thermal voltage or characteristic electric potential in the EDL, defined latter, $\psi_c \leq 25$ m V, and the surface tension between both fluids $\gamma_T \sim 10^{-3}$ N m^{-1}. With these values, the capillary number is estimated as $Ca \sim 10^{-4}$. Of course, for higher values of the surface tension, such as $\gamma_T \sim 10^{-2}$ N m^{-1}, the Capillary number is decreased, i.e, $Ca \sim 10^{-5}$. (iii) The net charge density in the two EDLs followed the well-known Boltzmann distribution. (iv) The Debye-Hückel approximation was considered. That is, at the liquid-wall surface interface and at the interface between both fluids, the zeta potentials were $\zeta_i \ll 25$ mV.

2.1 Mathematical Model

2.1.1 Electric Potential

Under the fore-mentioned assumptions, the Poisson equation that defines the electric potential ψ_i in each fluid is given by:

$$\frac{1}{r}\frac{d}{dr}\left(r\frac{d\psi}{dr}\right) = -\frac{\rho}{\varepsilon}, \quad i = 1,2, \tag{1}$$

where $\rho_{f,i}$ denotes the local charge density as given by the Boltzmann distribution

$$\rho = -2zen\,\sinh\left(\frac{ze\psi}{kT}\right), \quad i = 1,2. \tag{2}$$

In the analysis, the Debye-Hückel linearization was considered by assuming that $|ze\psi| \ll k_B T$, such that this could be expressed as follows: $\sinh(ze\psi/k_B T) \approx ze\psi/k_B T$ (i.e. $|\psi| \leq 0.025$ V) (Masliyah and Bhattacharjee 2006). Accordingly, with respect to small potentials, the linearized Poisson-Boltzmann equation is applied as follows:

$$\frac{1}{r}\frac{d}{dr}\left(r\frac{d\psi_i}{dr}\right) = K_i^2\psi_i, \quad i = 1,2. \tag{3}$$

Equation (3) are subject to the following boundary conditions:

$$\text{at } r = 0: \quad \frac{d\psi}{dr} = 0, \tag{4}$$

$$\text{at } r = R_1: \quad \psi_1 - \psi_2 = \Delta\psi, \tag{5}$$

$$\text{at } r = R_1: \quad \varepsilon_1\frac{\partial\psi_1}{\partial r} - \varepsilon_2\frac{\partial\psi_2}{\partial r} = -q_{sf} \tag{6}$$

and

$$\text{at } r = R_2: \quad \psi_2 = \zeta_w \tag{7}$$

Equation (4) represents the axisymmetric boundary condition, and Eq. (7) denotes the surface zeta potential, ζ_w, of the microcapillary wall. The zeta potential difference, $\Delta\psi$, at the interface between both fluids is represented by Eq. (5). Finally, the Gauss law, Eq. (6) was introduced into the electrical displacement of both fluids, where q_{sf} denotes the surface charge density at the liquid/liquid inter-face.

2.1.2 Flow Field

In order to determine the velocity profile, the steady-state modified Navier-Stokes equation was used for each fluid where the electric force is taken into account as follows:

$$0 = \mu_i\frac{1}{r}\frac{d}{dr}\left(r\frac{du_i}{dr}\right) + \rho_{f,i}E_0, \quad i = 1,2, \tag{8}$$

where μ_i denotes the dynamic viscosity. The boundary conditions associated with Eq. (8) include the following:

$$\text{at } r = 0: \quad \frac{du_1}{dr} = 0, \tag{9}$$

$$\text{at } r = R_1: \quad u_1 = u_2, \tag{10}$$

$$\text{at } r = R_1: \quad \mu_1\frac{du_1}{dr} - E_0\varepsilon_1\frac{d\psi_1}{dr} = \mu_2\frac{du_2}{dr} - E_0\varepsilon_2\frac{d\psi_2}{dr}. \tag{11}$$

$$\text{at } r = R_2: \quad u_2 = 0 \tag{12}$$

Boundary conditions (9)-(12) represent the condition of symmetry in the microcapillary, the continuity of velocities at the interface between both flu-ids, the balance of total stresses at the interface, and the no slip condition at the liquid/solid interface, respectively. It should be noted that the boundary condition (11) considered contributions from Maxwell as well as viscous stresses (Chang and Yeo 2009).

2.1.3 Dimensionless Governing Equations

In order to obtain the dimensionless version of the governing equations, the following non-dimensional variables are introduced: $\eta = r/R_1$, $Z = (r - R_1)/h$, $\bar{u}_i = u_i/u_c$, and $\bar{\psi}_i = \psi_i/\psi_c$. In previous definitions of non-dimensional variables, the characteristic velocity is given by the following expression: $u_c = \varepsilon_1 E_0 \psi_c / \mu_1$, where $\psi_c = k_B T / ze$ denotes the thermal voltage associated with the inner fluid. With respect to the above dimensionless variables, the governing equations (3) and (8) are transformed as follows:

for $0 \le \eta \le 1$:

$$\frac{1}{\eta}\frac{d}{d\eta}\left(\eta\frac{d\bar{\psi}_1}{d\eta}\right)=\bar{\kappa}_1^2\bar{\psi}_1 \tag{13}$$

over $0 \le Z \le 1$:

$$\frac{1}{Z+\varphi}\frac{d}{dZ}\left[(Z+\varphi)\frac{d\bar{\psi}_2}{d\eta}\right]=\bar{\kappa}_2^2\bar{\psi}_2 \tag{14}$$

for $0 \le \eta \le 1$:

$$0=\frac{1}{\eta}\frac{d}{d\eta}\left(\eta\frac{d\bar{u}_1}{d\eta}\right)+\bar{\kappa}_1^2\bar{\psi}_1 \tag{15}$$

and for $0 \le Z \le 1$:

$$0=\frac{d}{dZ}\left[\left(1+\frac{Z}{\varphi}\right)\frac{d\bar{u}_2}{dZ}\right]+\Upsilon\left(1+\frac{Z}{\varphi}\right)\bar{\kappa}_2^2\bar{\psi}_2. \tag{16}$$

The parameters that appear in Eqs. (13)-(16) are defined as follows: $\Upsilon=\varepsilon_r/\mu_r$, $\varphi=R_1/h$, $\bar{\kappa}_1=\kappa_1 R_1$, and $\bar{\kappa}_2=\kappa_2 h$, where $\varepsilon_r=\varepsilon_2/\varepsilon_1$ and $\mu_r=\mu_2/\mu_1$ denote permittivity and viscosity ratios of surrounding and inner fluids, respectively. The electrokinetic parameters $\bar{\kappa}_1$ and $\bar{\kappa}_2$ represent the ratio of the radius of the inner region to the Debye length formed at the interface and the ratio of the thick-ness of the surrounding fluid to the Debye length that forms at the solid-fluid interface, respectively. It should be noted that $\bar{\kappa}_2$ also represents the ratio of the surrounding fluid thickness to the Debye length that forms at the fluid-fluid interface on the surrounding fluid side.

Substituting the dimensionless variables into the boundary conditions (4)-(7) and (9)-(12), for the electric and velocity fields, yields the following expressions:

$$\frac{d\bar{\psi}_1(\eta=0)}{d\eta}=0, \tag{17}$$

$$\bar{\psi}_1(\eta=1)-\bar{\psi}_2(Z=0)=\Delta\bar{\psi}, \tag{18}$$

$$\frac{d\bar{\psi}_1(\eta=1)}{d\eta}-\varepsilon_r\varphi\frac{d\bar{\psi}_2(Z=0)}{dZ}=\varepsilon_r\varphi\bar{Q}_{sf}, \tag{19}$$

$$\bar{\psi}_2(Z=1)=\bar{\zeta}_w, \tag{20}$$

$$\frac{d\bar{u}_1(\eta=0)}{d\eta}=0, \tag{21}$$

$$\bar{u}_1(\eta=1)=\bar{u}_2(Z=0), \tag{22}$$

$$\frac{d\bar{u}_1(\eta=1)}{d\eta}-\frac{d\bar{\psi}_1(\eta=1)}{d\eta}=\varphi\left[\mu_r\frac{d\bar{u}_2(Z=0)}{dZ}-\varepsilon_r\frac{d\bar{\psi}_2(Z=0)}{dZ}\right] \tag{23}$$

and

$$\bar{u}_2(Z=1)=0. \tag{24}$$

In the above equations, the dimensionless surface charge density is defined as $\bar{Q}_{sf}=hq_{sf}/\varepsilon_2\psi_c$, where $\bar{\zeta}_w=\zeta_w/\psi_c$ denotes the dimensionless electric zeta potential of the microcapillary wall, and $\Delta\bar{\psi}=\Delta\psi/\psi_c$ denotes the dimensionless jump zeta potential at the interface.

2.2 Analytical Solution for the Electric Potential

In order to determine the electric potential distribution in both fluids, Eqs. (15) and (16) are expressed as follows:

$$\eta^2\frac{d^2\bar{\psi}_1}{d\eta^2}+\eta\frac{d\bar{\psi}_1}{d\eta}-\eta^2\bar{\kappa}^2\bar{\psi}_1=0 \tag{25}$$

and

$$u^2\frac{d^2\bar{\psi}_2}{du^2}+u\frac{d\bar{\psi}_2}{du}-u^2\bar{\kappa}_2^2\bar{\psi}_2=0 \tag{26}$$

where $u = Z + \varphi$. As observed, Eqs. (25) and (26) correspond to modified Bessel differential equations (Olver *et al.* 2010). The solutions of these equations after applying boundary conditions (17)-(20) are given by the following:

for $0 \le \eta \le 1$:

$$\bar{\psi}_1=\left[A_1I_0(\bar{\kappa}_2\varphi)+A_2K_0(\bar{\kappa}_2\varphi)+\Delta\bar{\psi}\right]\frac{I_0(\bar{\kappa}_1\eta)}{I_0(\bar{\kappa}_1)} \tag{27}$$

and for $0 \le \eta \le 1$:

$$\bar{\psi}_2=\left[-A_2K_0\left(\bar{\kappa}_2[1+\varphi]\right)+\bar{\zeta}_w\right]\frac{I_0\left[\bar{\kappa}_2(\varphi+Z)\right]}{I_0\left(\bar{\kappa}_2(1+\varphi)\right)}+\left\{\frac{\frac{\bar{\zeta}_w}{I_0\left(\bar{\kappa}_2(1+\varphi)\right)}A_3-\Delta\bar{\psi}I_1(\bar{\kappa}_1)+A_6}{A_4-\frac{K_0\left(\bar{\kappa}_2[1+\varphi]\right)}{I_0\left(\bar{\kappa}_2[1+\varphi]\right)}A_3+A_5}\right\}K_0\left[\bar{\kappa}_2(\varphi+Z)\right]. \tag{28}$$

Here, I_0 and K_0 denote zero-order modified Bessel functions of the first and second type (Olver *et al.* 2010), respectively, and the parameters A_i ($i = 1,...6$) are defined in the Appendix.

In the above expressions, I_1 represents the modified Bessel function of order 1 (Olver *et al.* 2010). Therefore, using Eqs. (27) and (28), the local volumetric net charge densities for fluids 1 and 2 are given by the following corresponding equations:

$$\bar{\rho}_{f1}=\bar{\kappa}_1^2\left[A_1I_0(\bar{\kappa}_2\varphi)+A_2K_0(\bar{\kappa}_2\varphi)+\Delta\bar{\psi}\right]\frac{I_0(\bar{\kappa}_1\eta)}{I_0(\bar{\kappa}_1)} \tag{29}$$

and

$$\bar{\rho}_{f2}=A_1\bar{\kappa}_2^2I_0\left[\bar{\kappa}_2(\varphi+Z)\right]+A_2\bar{\kappa}_2^2K_0\left[\bar{\kappa}_2(\varphi+Z)\right]. \tag{30}$$

2.3 Velocity Field

By integrating Eqs. (15) and (16) twice with respect to η and Z, respectively, and applying boundary conditions (21)-(24), it was easily shown that the velocity profiles in the inner and surrounding fluids are as follows:

over $0 \le \eta \le 1$:

$$\bar{u}_1 = -\left[A_1 I_0\left(\bar{\kappa}_2\varphi\right) + A_2 K_0\left(\bar{\kappa}_2\varphi\right) + \Delta\bar{\psi}\right]\frac{I_0\left(\bar{\kappa}_1\eta\right)}{I_0\left(\bar{\kappa}_1\right)} + \rho_1 \tag{31}$$

and on the region $0 \le Z \le 1$

$$\bar{u}_2 = \varphi\rho_2 \ln\left(\frac{Z}{\varphi}+1\right) + \rho_3 + \rho_4$$

$$+\frac{\rho_4}{2}\left\{A_2\bar{\kappa}_2 K_1\left[\bar{\kappa}_2\left(\varphi+Z\right)\right] - A_1\bar{\kappa}_2 I_1\left[\bar{\kappa}_2\left(\varphi+Z\right)\right]\right\}$$

$$+\rho_5\left\{A_2 K_0\left[\bar{\kappa}_2\left(\varphi+Z\right)\right] - A_1 I_0\left[\bar{\kappa}_2\left(\varphi+Z\right)\right]\right\}$$

$$-\Upsilon\left[A_1 I_0\left(\bar{\kappa}_2\left(\varphi+Z\right)\right) + A_2 K_0\left(\bar{\kappa}_2\left(\varphi+Z\right)\right)\right] \tag{32}$$

In the above equations, K_1 denotes the modified Bessel Function of order 1. The parameters involved in Eqs. (31) and (32) are presented in the Appendix.

The dimensionless volumetric flow rates of the inner, $\bar{Q}_1$, and surrounding, $\bar{Q}_2$, fluids can be obtained by integrating the velocity profiles given by Eqs. (31) and (32), as follows:

$$\bar{Q}_1 = \int_0^1 2\bar{u}_1\eta d\eta \tag{33}$$

and

$$\bar{Q}_2 = \frac{2}{\varphi}\int_0^1 \bar{u}_2\left(1+\frac{Z}{\varphi}\right)dZ, \tag{34}$$

in which $\bar{Q}_1 = Q_1 / Q_c$ and $\bar{Q}_2 = Q_2 / Q_c$, where Q_1 and Q_2 represent the dimensional volumetric flow rates for the inner and surrounding fluids, respectively. Additionally, $Q_c = \pi R_1^2 u_c$ denotes the characteristic volumetric flow rate.

By solving for the integrals defined in Eqs. (33) and (34), the volumetric flow rate of the inner fluid is obtained as follows:

$$\bar{Q}_1 = -2\left[\frac{A_1 I_0\left(\bar{\kappa}_2\varphi\right) + A_2 K_0\left(\bar{\kappa}_2\varphi\right) + \Delta\bar{\psi}}{I_0\left(\bar{\kappa}_1\right)}\right]\times$$

$$\left[\frac{I_1\left(\bar{\kappa}_1\right)}{\bar{\kappa}_1} + \rho_1\right], \tag{35}$$

Furthermore, with respect to fluid 2, the dimensionless volumetric flow rate $\bar{Q}_2$ has to be determined by numerically integrating Eq. (34). This was performed by using the trapezoidal rule (Hoffman and Frankel 2001).

3. RESULTS AND DISCUSSION

In this study, analytical solutions of the dimensionless electrical potentials and velocity distributions were derived in a purely EOF of two conducting immiscible Newtonian fluids inside a microcapillary. The results indicated that the EOF was con-trolled by several dimensionless parameters such as the viscosity ratio μ_r and permittivity ratio ε_r of inner and surrounding fluids, electrokinetic parameters (denoted as $\bar{\kappa}_1$ and $\bar{\kappa}_2$), dimensionless zeta potential difference at the interface between both flu-ids (denoted as $\Delta\bar{\psi}$), and the dimensionless inter-face charge density jump $\bar{Q}_{sf}$. In order to estimate the values of the dimensionless parameters involved in the analysis, values of the physical parameters were used that were previously used in the specialized literature that examined electroosmotic flows of two immiscible fluids. They were estimated by appropriately combining typical values of the physical parameters as shown in Table 1. In this table, the values of the EDLs thicknesses and permittivity were based on those used in a previous study (Liu *et al*. 2009), and the value of the interfacial potential jump was also based on an extant study (Wandlowski *et al*. 1995). It should be noted that in the present study since the Debye-Hückel approximation was assumed, the appropriate values of $\Delta\psi$ were used such that $\psi_1 \le 25$ mV.

Table 1 Typical values of physical parameters

Parameter	Value	units
R_1	10	μm
R_2	20	μm
L	~10^{-2}	m
E_0	~10^{4}	Vm^{-1}
ζ_w	<-25	mV
ε	8.854×10^{-12}	$Cm^{-1}V^{-1}$
ΔΨ	-130-190	mV
q_{sf}	0.015	Cm^{-2}
$\lambda_{D,i}$	30.2-302	nm

Figures 2 to 6 show the influence of the dimensionless parameters involved in the analysis of the electrical potential through the microcapillary as a function of the coordinates η and Z and the corresponding velocity profiles. It should be noted that in each of these figures, there is a gap in the potential electric distribution, which means that in domain the electric potential remains uniform and equal to zero. The effect of the jump dimensionless zeta potential at the liquid-liquid interface and the

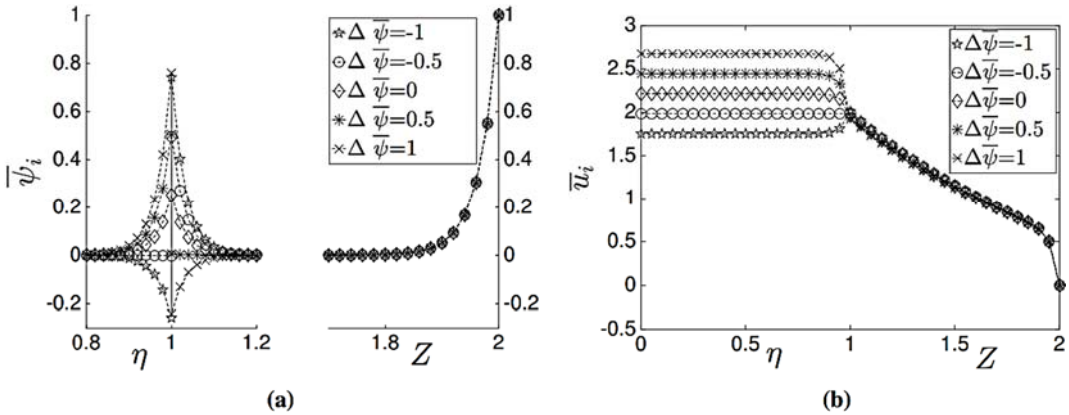

Fig. 2. (a) Electric potential distribution through the microcapillary for different values of the dimensionless jump zeta potential, and (b) the corresponding dimensionless velocity profiles. The following parameters were used: μ_r = 15, $\overline{\kappa}_1$ = 30, $\overline{\kappa}_2$ = 30, ε_r = 1 and $\overline{Q}_{sf}$ = 15.094, $\overline{\zeta}_w$ = 1.

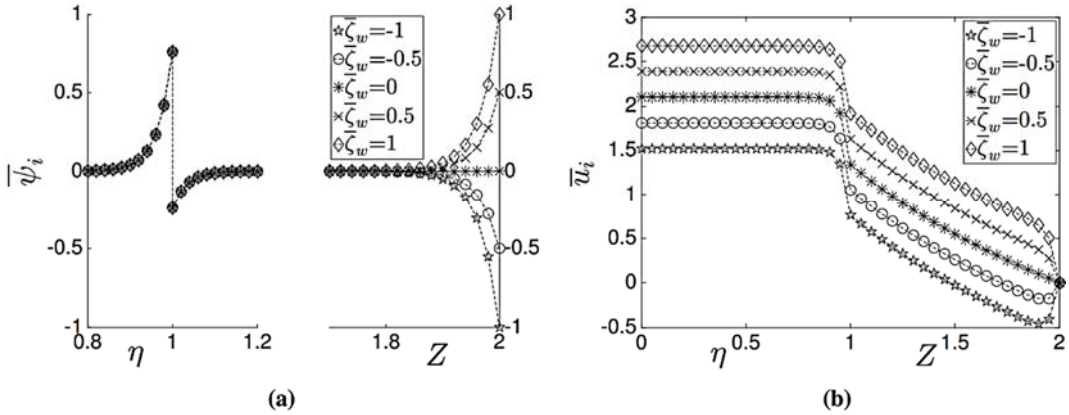

Fig. 3. (a) Electric potential distribution through the microcapillary for different values of the dimensionless zeta potential at the microcapillary wall, and (b) the corresponding dimensionless velocity profiles. The following parameters were used: μ_r = 15, $\overline{\kappa}_1$ = 30, $\overline{\kappa}_2$ = 30, $\Delta\overline{\psi} = 1$, ε_r = 1 and $\overline{Q}_{sf}$ = 15.094.

corresponding dimensionless velocity profiles are plotted in Figs. 2(a) and (b). It was observed that the presence of the surrounding fluid that acted as a lubricant increased the velocity of the inner fluid. Specifically, in the case of $\Delta\overline{\psi} = -1$, (line with the symbol ☆), the electric force in the inner fluid was opposite to that of the surrounding fluid at the interface between both fluids, and this slowed the net flow. In contrast, when $\Delta\overline{\psi} = 1$, , the velocity of the inner fluid corresponded to the maximum value due to a larger force at the liquid-liquid interface. This was because the zeta potential at the interface attained a value that could be evaluated from $\overline{\psi}_1(\eta = 1) = \Delta\overline{\psi} + \overline{\psi}_2(Z = 0)$. This in turn defined the zeta potential at the interface either in the inner or surrounding fluid side.

Figure 3 shows the effect of assuming negative and positive values of the dimensionless zeta potential of the microcapillary surface or its absence while maintaining a fixed zeta potential at the fluid-fluid interface. As observed in the figure, the electric potential distribution near the fluid-fluid interface was not modified due to the manner in which the wall was charged. Evidently, the jump zeta potential defined the behavior of the electrical potential distribution at the fluid-fluid interface. In this case, electrical forces in the inner fluid side at the fluid-fluid interface acted from the left to right as shown in Fig. 1, thereby dragging the surrounding fluid. However, with respect to $\overline{\zeta}_w < 0$, the electric force near the wall acted in a manner opposite to those developed in the inner fluid at the fluid-fluid interface. Therefore, the bulk velocity diminished as shown in the curves denoted as ◦ and ☆. In the case of $\overline{\zeta}_w = 0$ (a line denoted as ∗), the capillary wall was not electrically charged, and thus the surrounding fluid motion was analogous to that of a shear driven flow that was dragged by the inner fluid.

Figure 4(a) shows the plots of electric potential distribution for different values of the dimensionless interfacial charge density. As shown in the figure, the influence of the interfacial charge density was practically null. However, the effect of

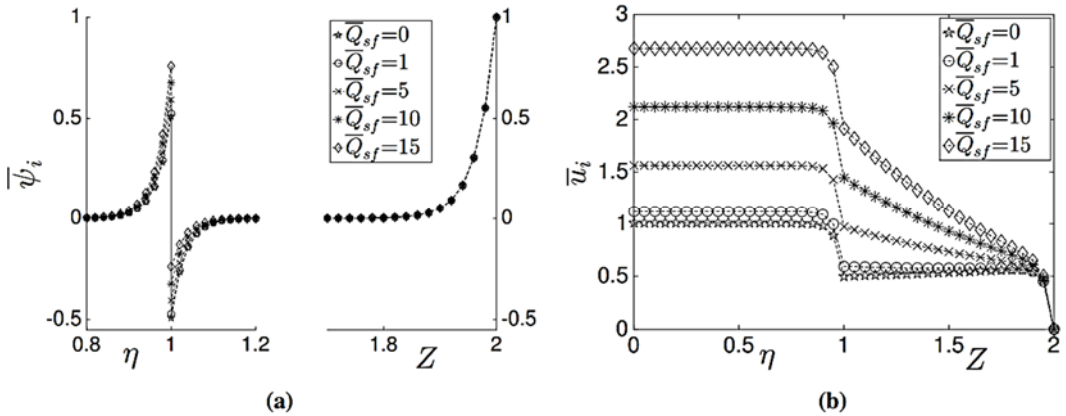

Fig. 4. (a) Electric potential distribution through the microcapillary for different values of the dimensionless surface-charge density, and (b) the corresponding dimensionless velocity profiles. The following parameters were used: $\mu_r = 15$, $\overline{\kappa}_1 = 30$, $\overline{\kappa}_2 = 30$, $\Delta\overline{\psi} = 1$, $\varepsilon_r = 1$, $\overline{\zeta}_w = 1$.

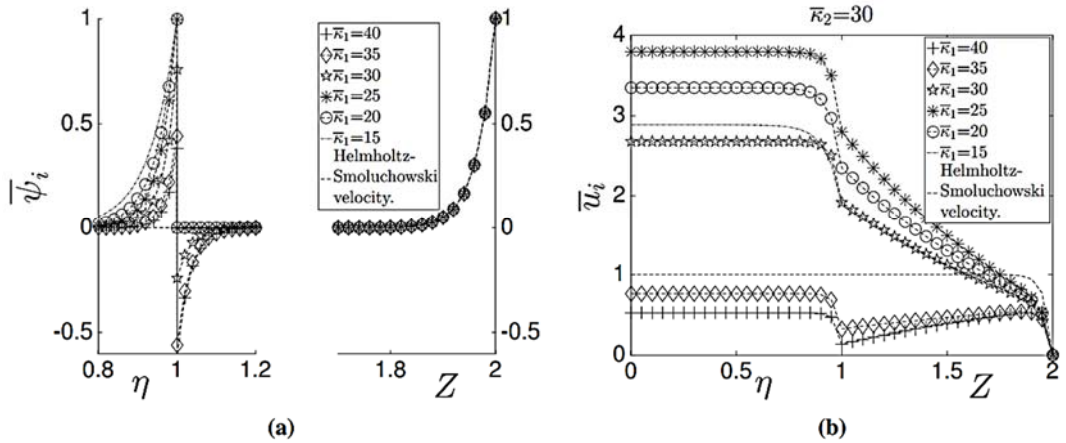

Fig. 5. (a) Electric potential distribution through the microcapillary for different values of the electrokinetic parameter $\overline{\kappa}_1$, and (b) the corresponding dimensionless velocity profiles. The following parameters were used: $\mu_r = 15$, $\overline{\kappa}_2 = 30$, $\Delta\overline{\psi} = 1$, $\varepsilon_r = 1$, $\overline{\zeta}_w = 1$ and $\overline{Q}_{sf} = 15.094$.

$\overline{Q}_s$ on the velocity profiles was particularly significant. As shown in Fig. 4(b), increasing values of $\overline{Q}_{sf}$ led to a significant increase in the velocity magnitudes of the inner fluid. The dimensionless surface-charge density assumed values of $0 \le \overline{Q}_{sf} \le 15$. In this direction, a value of $\overline{Q}_{sf} = 15$ was estimated with respect to the dimensional surface-charge density $q_{sf} = 0.0015$ C/m^2 (Choi *et al*. 2011). When $\overline{Q}_{sf} = 0$ the velocity of the inner fluid tends to the Helmholtz-Smoluchowski velocity.

The effect of the electrokinetic parameters $\overline{\kappa}_1$ and $\overline{\kappa}_2$ on electric and velocity distributions are shown in Figs. 5 and 6, respectively. Evidently, in both figures, the velocity profile exhibited a nonlinear behavior as the parameters $\overline{\kappa}_1$ or $\overline{\kappa}_2$ increased. For instance, in Fig. 5, with respect to values of $\overline{\kappa}_1$ = (15,20,25), the velocity magnitudes for both fluids increased and the velocity decreased for $\overline{\kappa}_1$ = 30. Similar behavior was observed in Fig. 6 with variations in the parameter $\overline{\kappa}_2$. Nevertheless, the effect of $\overline{\kappa}_2$ on the velocity when compared with that of $\overline{\kappa}_1$, was more significant because greater velocities were obtained. Evidently, the fore-mentioned observation was reflected in the volumetric flow rate as shown below. Additionally, when both fluids have the same physical properties, the well-known plug-like velocity profile is recovered, which is rep-resented by the dashed line in Fig. 5(b).

When both fluids have the same physical proper-ties, some of the dimensionless parameters involved in Eqs. (31) and (32) assumed the following values: $\mu_r = 1$, $\varepsilon_r = 1$ and $\Upsilon = 1$. Additionally, if the jump in the electrical potential and the charge density across the interface did not exist, $\Delta\overline{\psi} = 0$ and $\overline{Q}_{sf} = 0$. By considering the above, the velocity profiles for the inner and outer fluids as given by Eqs. (31) and (32) can be simplified and yields $\overline{u}_1 = 1$ and $\overline{u}_2 = 1 - I_0(\overline{\kappa}_2 Z) / I_0(\overline{\kappa}_2)$, respectively. Both

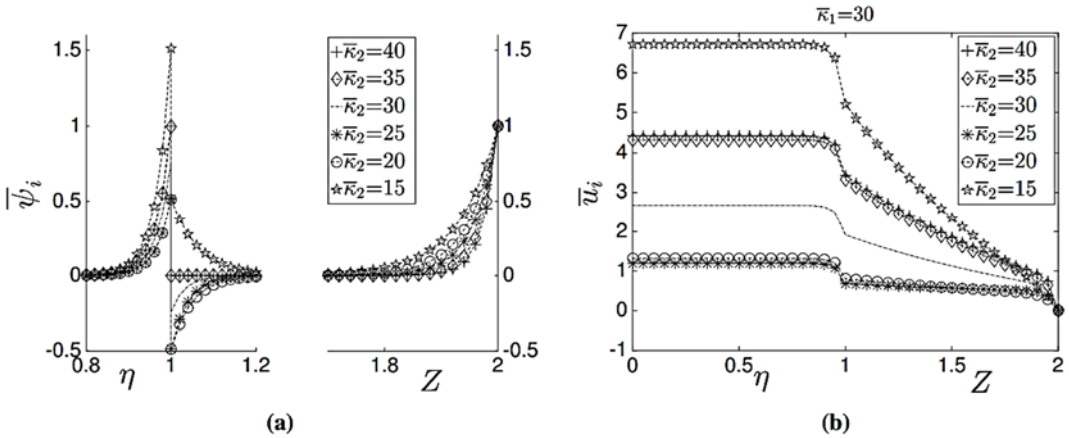

(a) **(b)**

Fig. 6. (a) Electric potential distribution through the microcapillary for different values of the electrokinetic $\bar{\kappa}_2$, and (b) the corresponding dimensionless velocity profiles. The following parameters were used: μ_r = 15, $\bar{\kappa}_1$ = 30, $\Delta\bar{\psi} = 1$, $\bar{\zeta}_w = 1$ and $\bar{Q}_{sf}$ = 15.094.

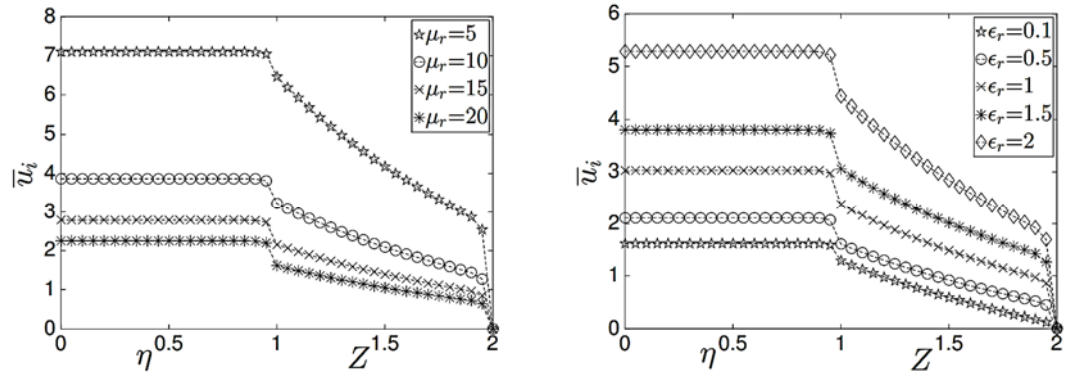

(a) **(b)**

Fig. 7. (a) Influence of the viscosity ratio and (b) permittivity ratio between the surrounding and inner fluids on the dimensionless velocity profiles. The following parameters were used: $\bar{\kappa}_1$ = 50, $\bar{\kappa}_2$ = 50, $\Delta\bar{\psi}$ =0.967, $\bar{\zeta}_w$ =1 and $\bar{Q}_{sf}$ = 13; in Fig 7(a), ε_r= 1 and in Fig. 7(b), μ_r= 15.

equations represent the solution to the electroosmotic flow of a single fluid in the circular capillary as represented by the dashed line in Fig. 5(b).

The effect of the viscosity ratio μr on the velocity profiles is shown in Fig. 7(a). The velocities for both fluids increased when the surrounding fluid was less viscous than the inner fluid. Figure 7(b) shows the influence of the parameter ε_r that depicts the competition between the dielectric permittivities of both fluids. It was observed that a higher velocity was attained when the surrounding fluid possessed increased permittivity. Additionally, $\varepsilon_r \rightarrow 0$, indicated that the surrounding fluid was electrically weakly conductive and that the fluid motion of the surrounding fluid was exclusively due to viscous forces that existed in the interface, which originated from the inner fluid. Analogously, the inner fluid was electrically weakly conductive when $\varepsilon_r \rightarrow \infty$, $\varepsilon_2 << \varepsilon_1$,.

Figure 8 shows the volumetric flow rates $\bar{Q}_i$ as a function of parameter (a) $\Delta\bar{\psi}$, (b) $\bar{\zeta}_w$, (c) $\bar{\varepsilon}_r$, (d) $\bar{\mu}_r$, (e) $\bar{\kappa}_1$, and (f) $\bar{\kappa}_2$. The influence of $\Delta\bar{\psi}$ on the volumetric flow rate of both immiscible fluids is shown in Fig. 8(a). In this case, as the dimensionless jump zeta potential increased, the volumetric flow rate of the surrounding fluid was slightly diminished and for the inner fluid was significantly increased. In Fig. 8(b), the volumetric flow rate of the two flu-ids varied linearly as a function of $\bar{\zeta}_w$. It was ob-served that with respect to the assumed values of the parameters, the volumetric flow rate is always an increasing function if the microcapillary wall was charged positive or negative, obtaining the best volumetric flow for the surrounding fluid when the zeta potential of the wall is $\zeta_w = 1$. The effect of permittivity ratio, ε_r, on the volumetric flow rate is shown in Fig. 8(c), where it was observed that the volumetric flow rate increases in a linear fashion for in-creasing values of the permittivity ratio. In contrast, the volumetric flow rates $\bar{Q}_i$ were diminished when the surrounding fluid had a greater viscosity when compared with that of the inner fluid, Fig. 8(d). An interesting characteristic of the

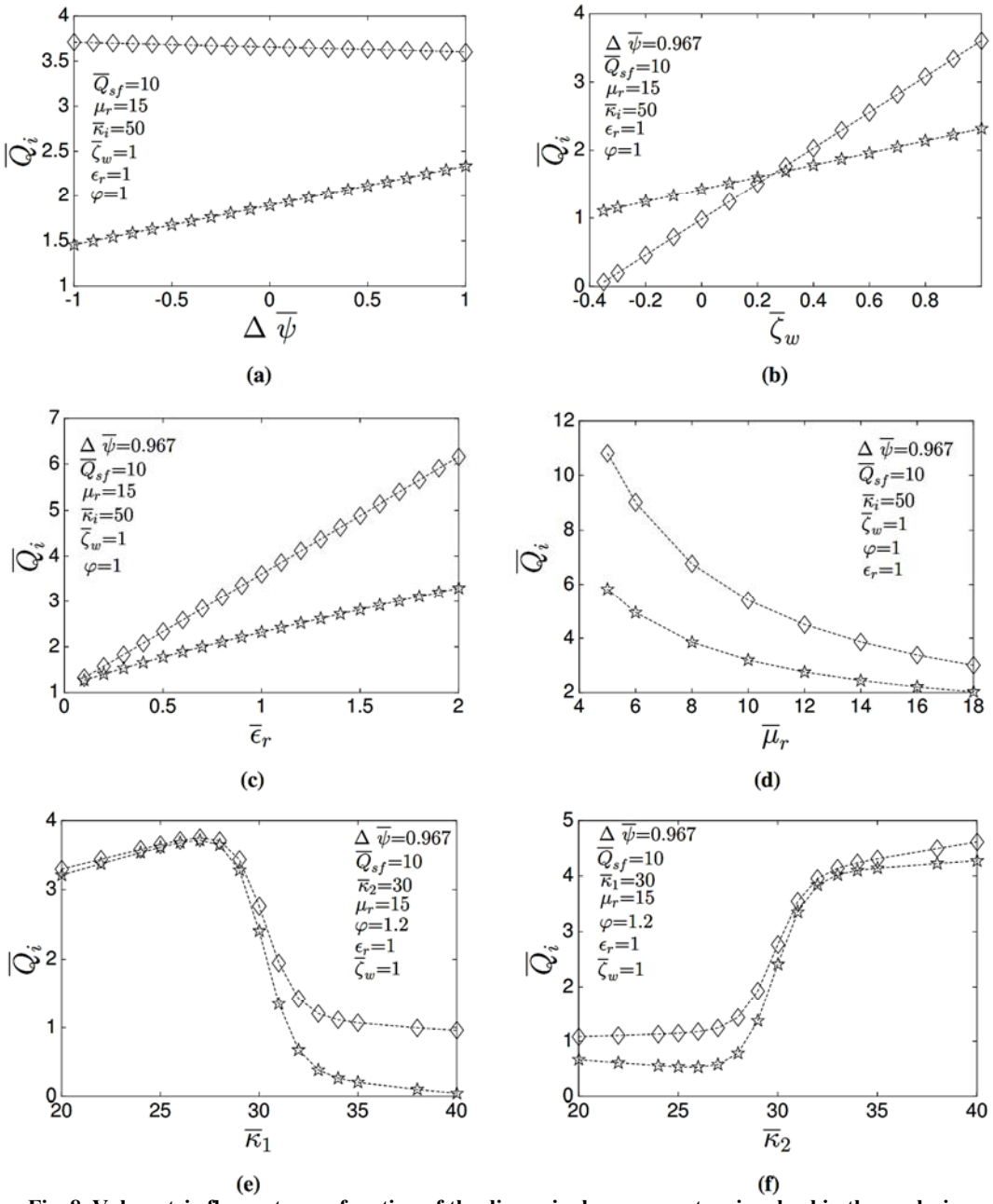

Fig. 8. Volumetric flow rate as a function of the dimensionless parameters involved in the analysis. Lines with the symbol ☆ represent the dimensionless volumetric flow rate of the inner fluid, while lines with the symbol ◊ correspond to the dimensionless volumetric flow rate of the surrounding fluid.

volumetric flow rates is shown in Figs. 8(e) and (f) which show the behavior of $\overline{Q}_i$ when the electrokinetic parameters $\overline{\kappa}_i$ are increased. In the former figure, maxima values for $\overline{Q}_i$ were observed when $\overline{\kappa}_i \approx 27$ for $\overline{\kappa}_2 = 30$. Conversely, with respect to $\overline{\kappa}_1 = 30$, the volumetric flow rates corresponded to a monotonic function for increasing values of $\overline{\kappa}_2$.

In Fig. 9 we show the behavior of velocity pro-files for greater values of $\overline{\kappa}_1$ and $\overline{\kappa}_2$ than those used in previous figures. As expected, for thin EDLs at the interface between both fluids, velocity profiles become fairly flat in the central region of the microchannel, and velocity gradients at the interface increase in a notable manner. The above is clearly appreciated by comparing, for example, Figs. 9(a) and 9(b) against Figs. 5(b) and 6(b). In Fig. 9(c) we show the effect when the inner fluid has a lower viscosity than that of the surrounding fluid, which is denoted by having values of $\mu_r < 1$. By comparing this figure against Fig. 7(a), the inner fluid reaches greater values than those obtained when $\mu_r > 1$.

Finally, the volumetric flow rate for values of the electrokinetic parameter $\overline{\kappa}_1 > 50$ and $\overline{\kappa}_2 > 100$ are shown in Figs. 10(a) and 10(b), respectively. As can

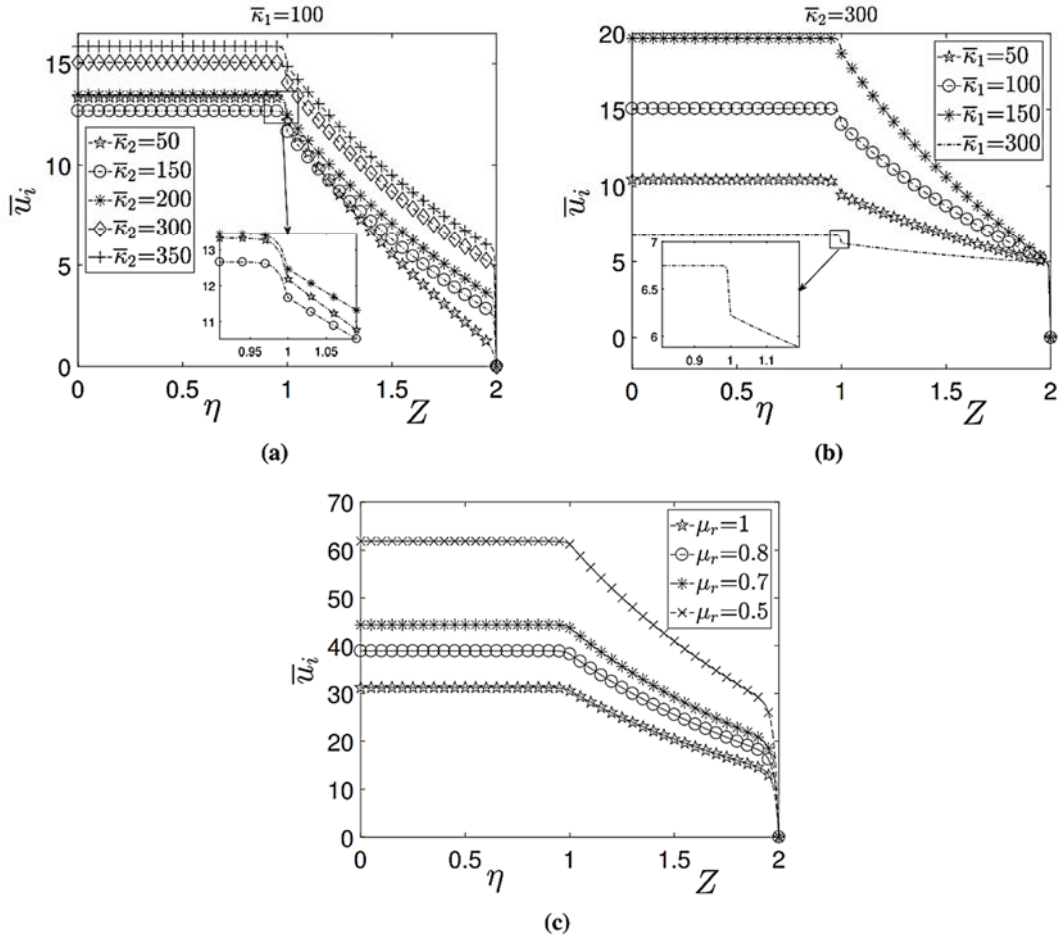

Fig. 9. Dimensionless velocity profiles as function of the coordinates η and Z, for values of (a) 50 < $\bar{\kappa}_2$ < 350, evaluated with $\bar{\kappa}_1$ = 100, and (b) 50 < $\bar{\kappa}_1$ < 300, evaluated with $\bar{\kappa}_2$ = 300. (c) Influence of the parameter $\mu_r \leq 1$ on the dimensionless velocity profiles. In figures (a) and (b), the values of the parameters that were considered are as follows: $\Delta\bar{\psi} = 1$, $\bar{Q}_{sf}$ = 15.094, μ_r = 15, $\bar{\varphi}$ =1, ε_r= 1 and $\bar{\zeta}_w$ =1. For Fig (c), $\Delta\bar{\psi} = 1$, $\bar{Q}_{sf}$ = 13, $\bar{\varphi}$ =1, ε_r= 1, $\bar{\zeta}_w$ =1, $\bar{\kappa}_1$ =50, $\bar{\kappa}_2$ =50.

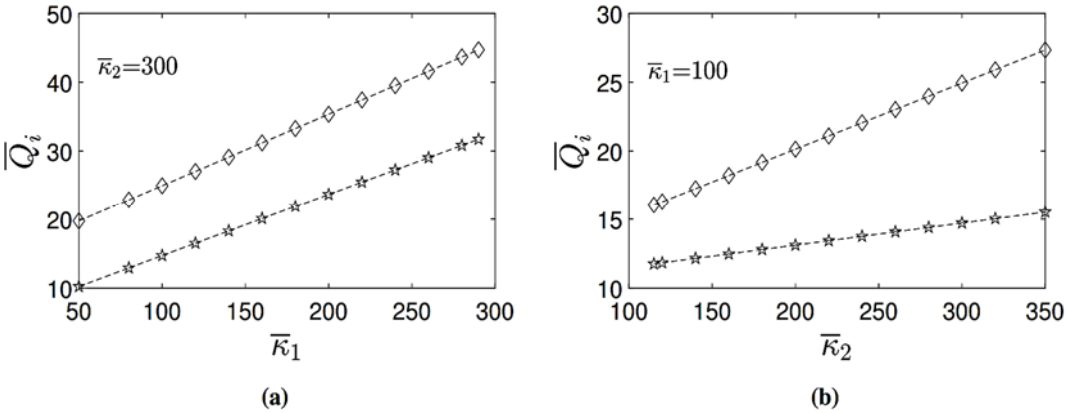

Fig. 10. Dimensionless volumetric flow rate, Qi with i = 1,2, as function of (a) $\bar{\kappa}_1$ > 50, evaluated with $\bar{\kappa}_2$ = 300 and (b) $\bar{\kappa}_2$ > 100, evaluated with $\bar{\kappa}_1$ = 100. Lines with the symbol ☆ represent the dimensionless volumetric flow rate of the inner fluid, while lines with the symbol ◊ correspond to the dimensionless volumetric flow rate of the surrounding fluid. Here, = 15.094, μr = 15, =1, εr= 1, =1.

be seen, the volumetric flow rate behaves in a linear fashion, in contrast to the behavior shown in Figs. 7(a) and 7(b), where relative low values of $\bar{\kappa}_1$ and

$\bar{\kappa}_2$ were assumed.

It should be noted that we have not shown the behavior of the other variables, such as the electric potential in the EDLs, for values of $\bar{\kappa}_i > 100$ with i = 1,2, because of the underlying mechanisms are similar as those described along the Result Section.

4. CONCLUSIONS

The present study involved an analytic study of the electro-osmotic flow in a microcapillary with two immiscible fluids, namely Newtonian as well as electrical conductors. The analysis accounted for viscous forces and electric stresses that acted at the interface between both fluids. The results demonstrated the importance of the formation of the EDL at the interface between both immiscible fluids. Additionally, the effect of the competition between the dynamic viscosity and permittivity of both fluids was observed via the dimensionless parameters μ_r and ε_r. Future studies will investigate the analysis of transient effects as well as thermal effects in these types of electroosmotic flows. Future research should also examine the relaxing of the assumption of a flat interface.

ACKNOWLEDGMENTS

This work was supported by the Fondo Sectorial de Investigación para la Educación through research grant no. CB-2013/220900 from SEP-CONACYT. Furthermore, O. Bautista acknowledges the partial support from SIP-IPN under contract number 20171181. A. Matías thanks the CONACYT program for a doctoral fellowship.

APPENDIX

The expressions for A_1-A_6 presented in Section 1.2 are the following:

$$A_1 = \frac{-A_2 K_0\left(\bar{\kappa}_2\left[1+\varphi\right]\right)+\bar{\zeta}_w}{I_0\left(\bar{\kappa}_2\left(1+\varphi\right)\right)},$$

$$A_2 = \frac{\dfrac{\bar{\zeta}_w}{I_0\left(\bar{\kappa}_2\left(1+\varphi\right)\right)}A_3 - \Delta\bar{\psi} I_1\left(\bar{\kappa}_1\right)+A_6}{A_4 - \dfrac{K_0\left(\bar{\kappa}_2\left[1+\varphi\right]\right)}{I_0\left(\bar{\kappa}_2\left[1+\varphi\right]\right)}A_3 + A_5}$$

$$A_3 = \left[-I_0\left(\bar{\kappa}_2\varphi\right)I_1\left(\bar{\kappa}_1\right)+\varepsilon_r\varphi I_1\left(\bar{\kappa}_1\varphi\right)I_0\left(\bar{\kappa}_1\right)\right],$$

$$A_4 = K_0\left(\bar{\kappa}_2\varphi\right)I_1\left(\bar{\kappa}_1\right),$$

$$A_5 = \varepsilon_r\varphi K_1\left(\bar{\kappa}_1\varphi\right)I_0\left(\bar{\kappa}_1\right),$$

$$A_6 = \frac{\varepsilon_r\varphi\bar{Q}_{sf}I_0\left(\bar{\kappa}_1\right)}{\bar{\kappa}_1}.$$

The expressions for ρ_1-ρ_5 presented in Section 1.2 are the following:

$$\rho_1 = -\Upsilon\Pi_4 + \Upsilon\varphi\left[\ln\left(\varphi\right)\right]^2\left(1-\frac{\Pi_6}{2}\right) + \left\{A_1 I_0\left(\bar{\kappa}_2\varphi\right)+A_2 K_0\left(\bar{\kappa}_2\varphi\right)+\Delta\bar{\psi}\right\} + \frac{\varphi\Upsilon\Pi_5}{\left(1-\dfrac{1}{\varphi\bar{\kappa}_2}\right)}+\rho_3,$$

$$\rho_2 = \Upsilon\left\{\Pi_6\left[1-\ln\left(\varphi\right)\right]-\frac{2\Pi_4}{\varphi}\right\}+\frac{\varepsilon_r\Pi_6}{\mu_r} - \frac{2\bar{\kappa}_1 I_1\left(\bar{\kappa}_1\right)}{\mu_r\varphi}\left\{\frac{A_1 I_0\left(\bar{\kappa}_2\varphi\right)+A_2 K_0\left(\bar{\kappa}_2\varphi\right)+\Delta\bar{\psi}}{I_0\left(\bar{\kappa}_1\right)}\right\}$$

$$\rho_3 = \Upsilon\Pi_1 - \Upsilon\varphi\left[\ln\left(1+\varphi\right)\right]^2\left(1-\frac{\Pi_3}{2}\right) - \frac{\varphi\Upsilon\Pi_2}{\left(1-\dfrac{1}{\varphi\bar{\kappa}_2}\right)\left(\dfrac{1}{\varphi}+1\right)} - \rho_2\ln\left(1+\varphi\right),$$

$$\rho_4 = \Upsilon\varphi\left[\ln\left(Z+\varphi\right)\right]^2$$

And

$$\rho_5 = \frac{\Upsilon}{\left(1-\dfrac{1}{\varphi\bar{\kappa}_2}\right)\left(\dfrac{Z}{\varphi^2}+\dfrac{1}{\varphi}\right)}$$

where the parameters Π_1-Π_6 are defined as follows:

$$\Pi_1 = A_1 I_0\bar{\kappa}_2\left(1+\varphi\right)+A_2 K_0\bar{\kappa}_2\left(1+\varphi\right)$$

$$\Pi_2 = A_2 K_0\left[\bar{\kappa}_2\left(1+\varphi\right)\right]-A_1 I_0\left[\bar{\kappa}_2\left(1+\varphi\right)\right]$$

$$\Pi_3 = A_1\bar{\kappa}_2 I_1\left[\bar{\kappa}_2\left(1+\varphi\right)\right]-A_2\bar{\kappa}_2 K_1\left[\bar{\kappa}_2\left(1+\varphi\right)\right],$$

$$\Pi_4 = A_1 I_0\left(\bar{\kappa}_2\varphi\right)+A_2 K_0\left(\bar{\kappa}_2\varphi\right)$$

$$\Pi_5 = A_2 K_0\left(\bar{\kappa}_2\varphi\right)-A_1 I_0\left(\bar{\kappa}_2\varphi\right),$$

and

$$\Pi_6 = A_1\bar{\kappa}_2 I_1\left(\bar{\kappa}_2\varphi\right)-A_2\bar{\kappa}_2 K_1\left(\bar{\kappa}_2\varphi\right).$$

REFERENCES

Brask, A., G. Goranovic and H. Bruus (2003). Electroosmotic pumping of nonconducting liquids by viscous drag from a secondary conducting liquid. *Tech Proc Nanotech 1*, 190–193.

Chang, H. C. and L. Y. Yeo (2009). *Electrokinetically-Driven Microfluidics and Nanofluidics*. Cambridge University Press.

Choi, W., A. Sharmaa, S. Qian, G. Lim and S. W. Joo (2011). On steady two-fluid electroosmotic flow with full interfacial electro-statics. *J. Colloid Interface Sci. 357*, 521–526.

Gao, Y., T. N. Wong, C. Yang and K. T. Ooi (2005). Two-fluid electroosmotic flow in microchannels. *J. Colloid Interface Sci. 284*, 306–314.

Hoffman, J. D. and S. Frankel (2001). *Numerical Methods for Engineers and Scientists* (2nd ed.). CRC Press.

Jabari, A. (2016). Two-fluid Electrokinetic Flow in a Circular Microchannel. IJE TRANSACTIONS A: *Basics 29*(10), 1469–1477.

Kirby, B. J. (2010). *Micro and Nanoscale Fluid Mechanics*. Cambridge University Press.

Liu, M., Y. Liu, Q. Guo and J. Yang (2009). Modeling of electroosmotic pumping of nonconducting liquids and biofluids by a two-phase flow method. *J Electroanal. Chem. 636,* 86–92.

Mandal, S., U. Ghosh, A. Bandopadhyay and S. Chakraborty (2015). Electro-osmosis of superimposed fluids in the presence of modulated charged surfaces in narrow confinements. *J. Fluid Mech. 776,* 390–429.

Masliyah, J. H. and S. Bhattacharjee (2006). *Electrokinetic and Colloid Transport Phenomena*. Wiley-Interscience.

Matías, A., F. Méndez and O. Bautista (2017) Interfacial electric effects on a Non-isothermal Electroosmotic Flow in a Micro-capillary Tube Filled by Two Immiscible *Fluids. Micromachines 8*(8), 232.

Middleman, S. (1995). *Modeling Axisymmetric Flows: Dynamics of Films, Jets, and Drops*. Academic Press.

Movahed, S., S. Khani, J. Z. Wen and D. Li (2012) Electroosmotic flow in a water column sunrrounded by an immiscible liquid. *J. Colloid Interface Sci. 372,* 207–211.

Olver, F. W. J., D. W. Lozier, R. F. Boisvert and C. W. E. Clark (2010). NIST Handbook of Mathematical Functions. NIST Handbook of Mathematical Functions; print companion to (DLMF 2016).

Pascall, A. J. and T. M. Squires (2011). Electrokinetics at liquid/liquid interfaces. *J. Fluid Mech. 684,* 163–191.

Probstein, R. F. (2005*). Physicochemical Hydrodynamics: An Introduction*. John Wiley.

Qi, C. and C. O. Ng (2018). Electroosmotic flow of a two-layer fluid in a slit channel with gradually varying wall shape and zeta potential. *International Journal of Heat and Mass Transfer 119*, 52–64.

Su, J., Y. J. Jian, L. Chang and Q. S. Liu) Transient electro-osmotic and pres-sure driven(2013) flow of two-layer fluids through a slit microchannel. *Acta Mech. Sin. 29*(4), 534–542.

Verway, E. J. W. and K. F. Niessen (1939). The electrical double layer at the interface of two liquids. *Philosophical Magazine 28*, 435–446.

Volkov, A. G., D. W. Deamer, D. L. Tanelian and V. S. Markin (1996). Electrical double layers at the oil/water interface. *Progress in surface science 53*(1), 1–134.

Wandlowski, T., K. Holub, V. Marecek and Z. Samec (1995). The double layer at the interface between two immiscible electrolyte solutions—iv. solvent effect. Electrochemica *Acta 40(18),* 2887–2895.